Journal of Mechanics, 2022, **38**, 32–43
https://doi.org/10.1093/jom/ufac005
Regular Article

Cost-effective and accurate interlaminar stress modeling of composite Kirchhoff plates via immersed isogeometric analysis and equilibrium

Alessia Patton[1], Massimo Carraturo[1], Ferdinando Auricchio[1] and Alessandro Reali[1,*]

[1]Department of Civil Engineering and Architecture, University of Pavia, Pavia, Italy

*Corresponding author: alessandro.reali@unipv.it

ABSTRACT

The interest for composites has constantly grown in recent years, especially in the aerospace and automotive industries, as they can be moulded in complex form and geometry, as well as exhibit enhanced engineering properties. Nevertheless, despite the accelerated diffusion of laminated composites, the design of these materials is often restrained by the lack of cost-effective modeling techniques. In fact, the existing numerical strategies allowing for cheap simulations of laminated structures usually fail to directly capture out-of-plane through-the-thickness stresses, which are typically responsible for failure modes such as delamination. In this context, a stress recovery approach based on equilibrium has been recently shown to be an efficient modeling strategy in the framework of isogeometric analysis. Since immersed approaches like the finite cell method have been proven to be a viable alternative to mesh-conforming discretization for dealing with complex/dirty geometries as well as trimmed surfaces, we herein propose to extend the stress recovery approach combining the finite cell method, isogeometric analysis and equilibrium to model the out-of-plane behavior of Kirchhoff laminated plates. Extensive numerical tests showcase the effectiveness of the proposed approach.

KEYWORDS: laminated composites, isogeometric analysis, finite cell method, stress recovery

1 INTRODUCTION

Traditional computer-aided engineering (CAE) procedure starts from the geometry of a structure designed within a computer-aided design (CAD) environment. To evaluate stresses and other quantities of interest in the structure, CAE's workflow requires to generate a mesh, i.e. a discretized version of the original (exact) geometry, suitable to perform finite element analysis (FEA). However, when considering complex geometrical entities, such a mesh generation procedure turns out to be the actual bottleneck in the CAE process [1], since it is often hard to automatize and time consuming.

Isogeometric analysis (IgA) was initially proposed to overcome the mesh generation burden in structural analysis [2]. The idea is to employ the same functions used in CAD environments to represent geometrical entities (B-splines and Non-Uniform Rational B-splines (NURBS)) as basis functions for the analysis. Such an approach has demonstrated to have excellent properties which can be exploited in many mathematical and engineering applications [3–5]. In fact, the higher inter-element continuity that can be achieved by using B-splines basis functions yields a higher accuracy per degree of freedom (DOF) compared to standard Lagrange polynomials. Moreover, it allows to directly solve higher-order variational problems such as Kirchhoff-Love plates and shells [6–8].

However, when we have to deal with trimmed surfaces, "dirty" geometries as well as volumetric mesh generations, the traditional IgA approach might show problems similar to classical FEA. Therefore, immersed boundary approaches have been extensively studied in this context and have shown to be a valid alternative to mesh-conforming methods [9–11]. In particular, the finite cell method (FCM) [12, 13] seems to be a simple yet effective immersed boundary approach that can be easily combined together with IgA (FCM-IgA), as extensively shown in the literature [14–16].

Many other techniques can be found in the literature belonging to the family of the immersed boundary methods, for instance: the immersed boundary method by Peskin [17], the immersed boundary finite volume method [18], the fat-boundary method [19], XFEM [20], and CutFEM [21]. In particular, in this context, we recall the immersogeometric analysis method that has been successfully employed in fluid and fluid-structure interaction (FSI) simulations [22, 23]. Such a method inherits its main features from the IgA version of the FCM but it has been further specialized to deal with FSI and fluid problems [24–26]. Another very recently introduced method is the so-called Immersed Boundary-Conformal Method [27]. It takes advantage of both immersed and boundary conform approaches featuring a layer of conforming mesh and a background immersed boundary discretization using the minimal stabilization method introduced in [28]. Another interesting immersed-boundary/IgA computational framework for FSI can be finally found in [29].

Received: 29 December 2021; **Accepted:** 22 January 2022

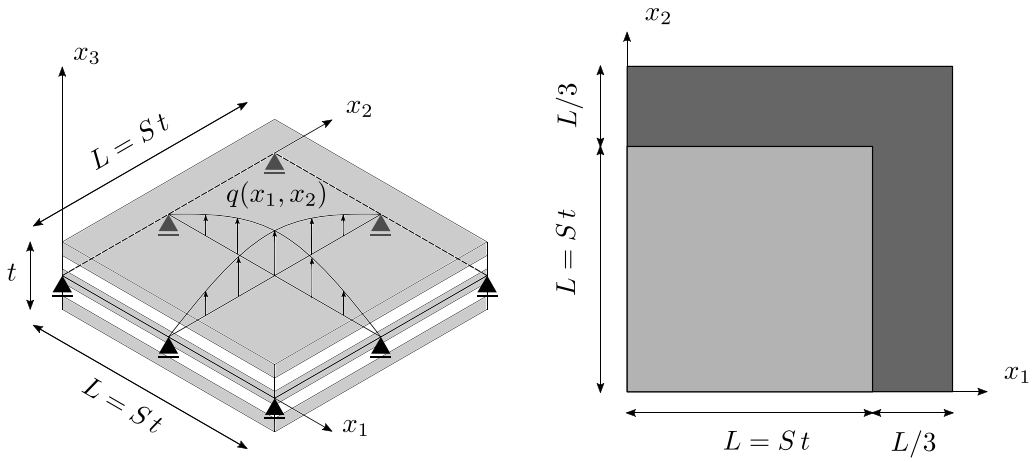

(a) Multi-layered conforming plate.

(b) Immersed *versus* conforming geometry.

Figure 1 Pagano's problem setup.

Table 1 Pagano's benchmark parameters.

Parameter	Value [unit]
Slenderness (S)	50 [-]
Thickness (t)	11 [mm]
Length (L)	550 [mm]

Table 2 Material parameters.

E_1	E_2	E_3	G_{23}	G_{13}	G_{12}	ν_{23}	ν_{13}	ν_{12}
[GPa]	[GPa]	[GPa]	[GPa]	[GPa]	[GPa]	[-]	[-]	[-]
25 000	1000	1000	200	500	500	0.25	0.25	0.25

Composite materials [30, 31] have attracted a lot of attention especially for aerospace applications, as they can in fact be moulded in various shapes and assembled in a multitude of lay-up arrangements. Therefore, the design process of those materials faces rather complex challenges comprising shape optimization, material compositions, architectures, and manufacturing [32]. For example, in laminated composites each ply exhibits a preferred high-strength direction, which can be tuned according to the fiber orientation, thereby giving designers the flexibility to tailor engineering properties of interest, such as laminate stiffness and strength, while still maintaining a reduced weight and matching even demanding structural requirements. Nevertheless, it is a well-known fact that laminated composites are prone to damage even under simple loading conditions due to a comparatively poorer strength in the out-of-plane direction as they typically exhibit a mismatch of material properties in different layers [33]. As a result, between two adjacent plies an interface crack might grow eventually leading to delamination [34]. Therefore, to properly assess the structural response of laminated structures, an accurate evaluation of the out-of-plane stress state is of paramount importance.

Standard approaches for the simulation of the behavior of laminated plates/shells consist, in general, of two-dimensional theories (such as the equivalent single-layer (ESL) approach [31]) and layerwise (LW) theories (see, e.g. [35–38]). In particular, LW theories typically show a comparatively higher computational cost with respect to ESL theories, especially for stacking sequences comprising a significant number of plies. However, the existing strategies allowing for cheap simulations, like the ESL approach, usually fail to directly capture out-of-plane through-the-thickness stresses.

The high smoothness achievable by IgA functions guarantees superior approximation properties and opens the door to the discretization of high-order partial differential equations in primal form, such as in the classical laminated plate theory (CLPT). In this study, we consider a displacement-based CLPT approach, which provides the lowest computational cost among known literature strategies, within an FCM-IgA framework that allows us to break away from the complexity of the geometry and possible complications in the meshing procedure. According to the CLPT, out-of-plane stresses are neglected, while in the case of cross-ply laminates weaker material strength properties in the stacking sequence cause stress concentrations at the interface level, eventually leading to premature failure. Nevertheless, interlaminar stresses may be recovered coupling the obtained displacement solution with a post-processing technique that directly imposes equilibrium equations [39]. As this *a posteriori* approach involves high-order in-plane derivatives, IgA represents a natural simulation framework given its high continuity properties and excellent accuracy-to-efficiency ratio. The adopted post-processing technique takes its origin in [40–42] and has already been proven to provide good results for 3D solid plates and shells in the context of both IgA Galerkin [43] and collocation [8, 44] methods (but also of finite element methods combined with Radial Basis Functions [45]).

The present work is structured as follows. Section 2 recalls the main concepts beneath the IgA stress recovery procedure first introduced in [39]. In Section 3, the interlaminar stress reconstruction approach is extended to an immersed formulation by means of the FCM. In Section 4, we present and discuss the results obtained adopting the presented numerical framework on two classical benchmarks: the Pagano's plate problem and the

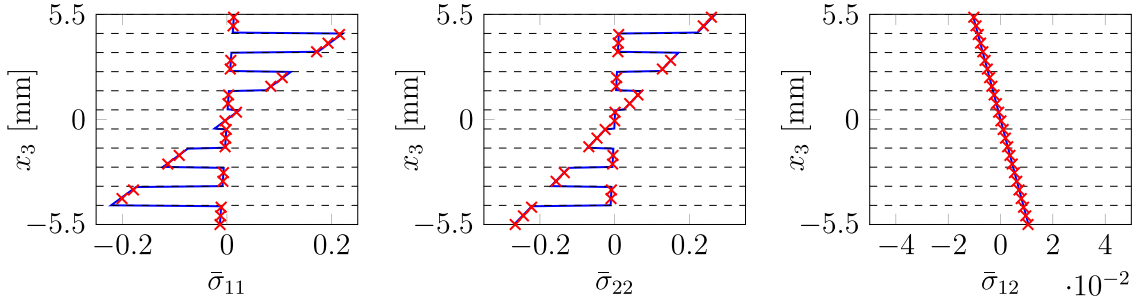

Figure 2 Through-the-thickness in-plane stress profiles at $x_1 = x_2 = 0.25\,L$. L represents the total length of the plate, that for this case is $L = 550$ mm (being $L = S\,t$ with $t = 11$ mm and $S = 50$), while the number of layers is 11 (—— Pagano's analytical solution [49] *versus* × FCM-IgA solution obtained with degree of approximation $p = q = 4$ and 14×14 knot spans).

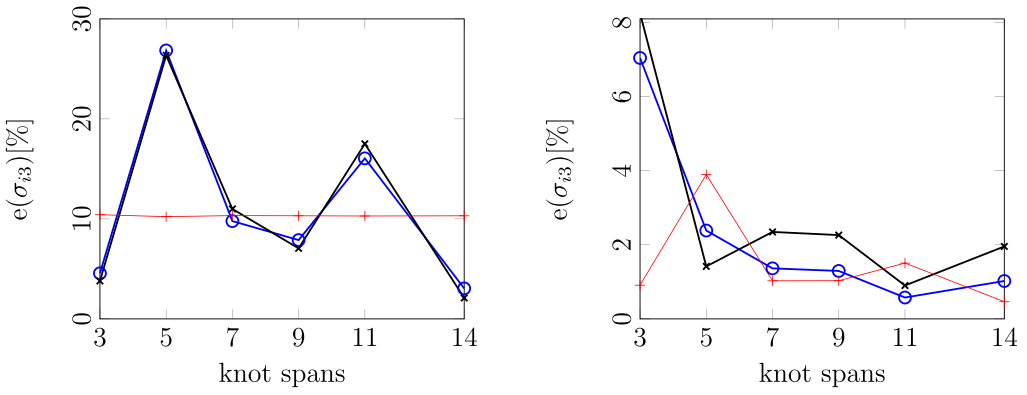

(a) 11 layers, $S = 50$, $p = q = 3$

(b) 11 layers, $S = 50$, $p = q = 4$

(c) 11 layers, $S = 50$, $p = q = 6$

Figure 3 L^2 relative percentage error evaluation (e(σ_{i3})[%], $i = 1, 2, 3$) at $x_1 = x_2 = 0.25\,L$. Different number of knot spans (i.e. 3×3, 5×5, 7×7, 9×9, 11×11, 14×14) are investigated for a number of layers equal to 11 and $S = 50$ (e(σ_{13})[%] —o—, e(σ_{23})[%] —×—, e(σ_{33})[%] —+—).

quarter of annulus problem. Finally, in Section 5, we draw the main conclusions of the present contribution.

2 LAMINATED COMPOSITE STRESS RECOVERY

The stress-recovery for conforming IgA laminated plates in linear elasticity may be regarded as a two-step procedure. First the usual balance of linear momentum is solved adopting a displacement-based CLPT[1] which features homogenized material properties of the stacking sequence of the composite according to [46]. This allows to obtain an immediate assessment of the in-plane stress state only using the constitutive equations. In fact, due to the kinematic assumptions in Kirchhoff's theory, out-of-plane stresses are identically zero. Then, starting from the

[1] We restrict our analysis to symmetric cross-ply laminates, thereby neglecting bending-stretching coupling coefficients and bending-twisting contributions. However, the proposed modeling approach provides reasonable approximations to more complex laminates such as antisymmetric cross-ply laminates [39].

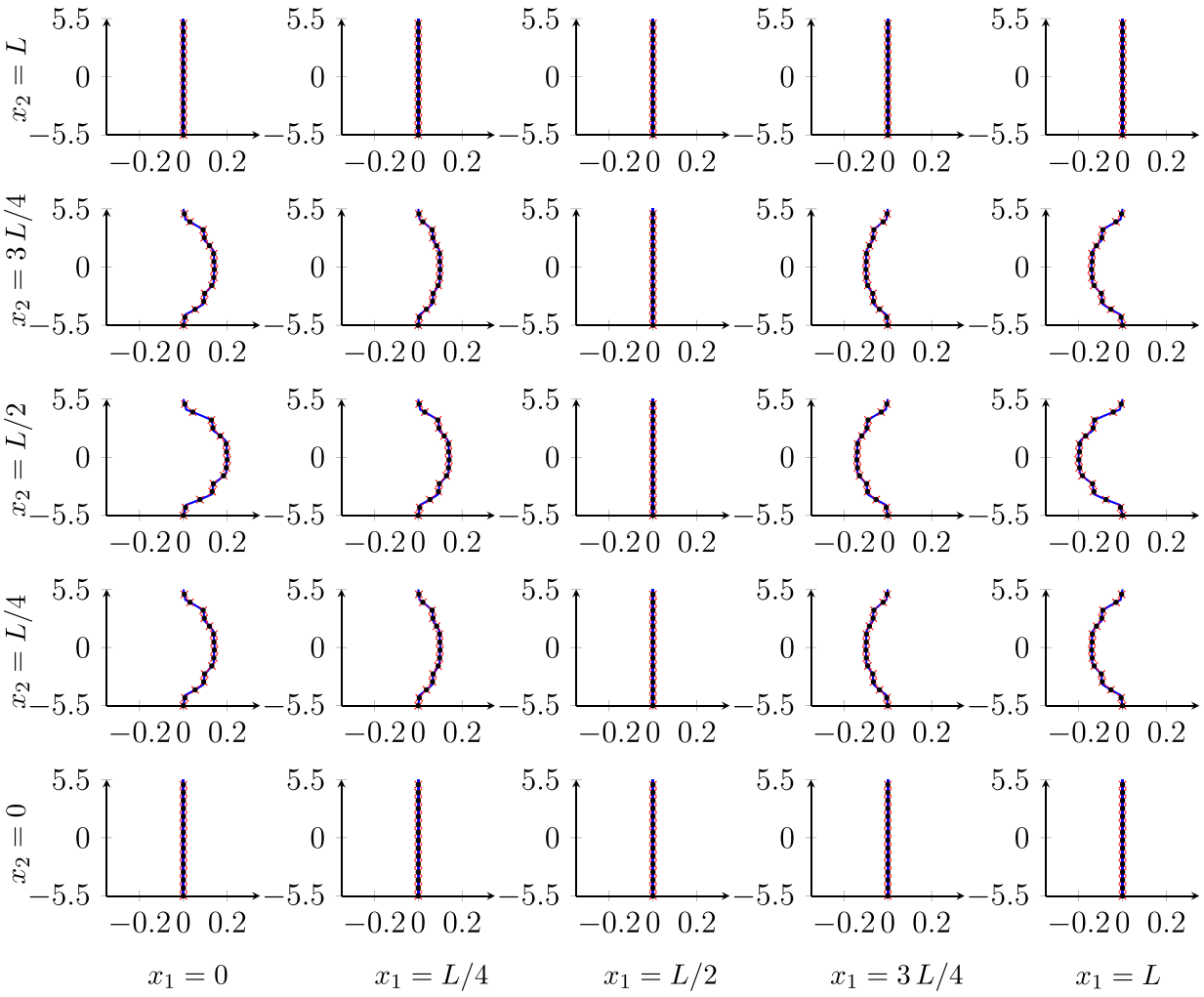

Figure 4 Through-the-thickness $\bar{\sigma}_{13}$ profiles for several in-plane sampling points. L represents the total length of the plate, that for this case is $L = 550$ mm (being $L = St$ with $t = 11$ mm and $S = 50$), while the number of layers is 11 (—— Pagano's analytical solution [49] *versus* recovered numerical solutions obtained with degree of approximation $p = q = 4$, and 14×14 knot spans: × FCM-IgA, • conforming IgA).

obtained transverse displacement solution w (even a coarse one), we can compute *a posteriori* the necessary high order derivatives of the in-plane stresses relying on the properties of the shape functions and impose equilibrium equations which allow for an accurate description also of the interlaminar stress state of the composite through the thickness.

Thus, if the considered deformable body is in equilibrium, stresses must satisfy the following equations:

$$\sigma_{11,1} + \sigma_{12,2} + \sigma_{13,3} = -b_1, \tag{1a}$$

$$\sigma_{12,1} + \sigma_{22,2} + \sigma_{23,3} = -b_2, \tag{1b}$$

$$\sigma_{13,1} + \sigma_{23,2} + \sigma_{33,3} = -b_3, \tag{1c}$$

where in Eqs. (1a)–(1c) and hereinafter we adopt the convention that the portion of a subscript prior to a comma indicates the components of a tensor, while the portion after the comma refers to partial derivatives; e.g. $\sigma_{13,3} = \frac{\partial \sigma_{13}}{\partial x_3}$.

Following [39, 43], an accurate solution can be obtained not only in terms of in-plane displacements and stresses, but also of derivatives of in-plane stresses with respect to in-plane coordinates. Therefore, the out-of-plane derivatives of the stress components in system (1) are decoupled from the in-plane ones. As a result, we can reformulate (1) in terms of interlaminar stresses, which we numerically integrate along the plate thickness coordinate ζ using a composite trapezoidal quadrature rule as

$$\sigma_{13}(x_3) = -\int_{\bar{x}_3}^{x_3} (\sigma_{11,1}(\zeta) + \sigma_{12,2}(\zeta) + b_1(\zeta))\mathrm{d}\zeta + \sigma_{13}(\bar{x}_3), \tag{2a}$$

$$\sigma_{23}(x_3) = -\int_{\bar{x}_3}^{x_3} (\sigma_{12,1}(\zeta) + \sigma_{22,2}(\zeta) + b_2(\zeta))\mathrm{d}\zeta + \sigma_{23}(\bar{x}_3), \tag{2b}$$

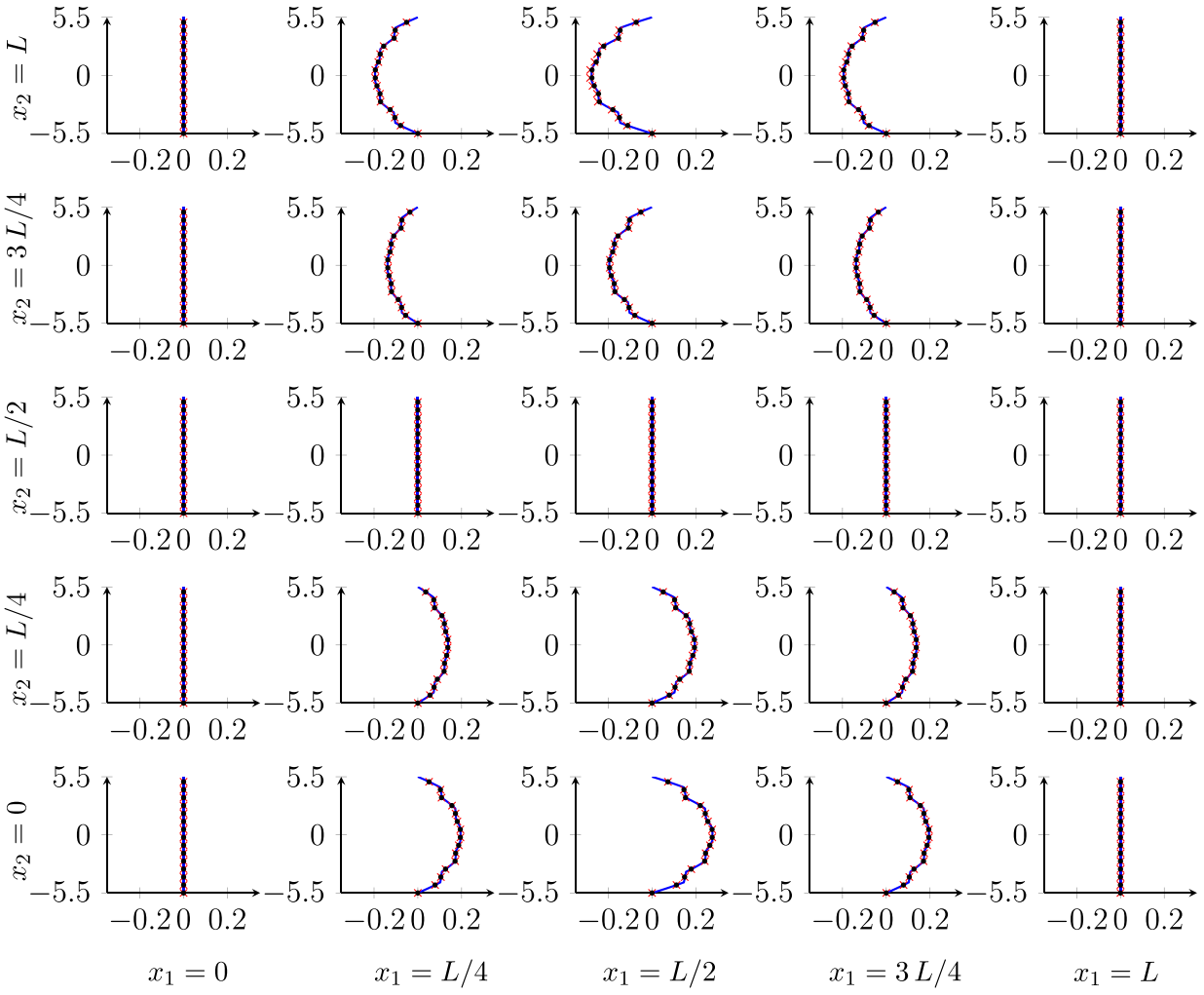

Figure 5 Through-the-thickness $\bar{\sigma}_{23}$ profiles for several in-plane sampling points. L represents the total length of the plate, that for this case is $L = 550$ mm (being $L = St$ with $t = 11$ mm and $S = 50$), while the number of layers is 11 (—— Pagano's analytical solution [49] *versus* recovered numerical solutions obtained with degree of approximation $p = q = 4$, and 14×14 knot spans: × FCM-IgA, • conforming IgA).

$$\sigma_{33}(x_3) = \int_{\bar{x}_3}^{x_3} \left[\int_{\bar{x}_3}^{\zeta} (\sigma_{11,11}(\xi) + \sigma_{22,22}(\xi) + 2\sigma_{12,12}(\xi) + b_{1,1}(\xi) + b_{2,2}(\xi))\mathrm{d}\xi \right] \mathrm{d}\zeta - \int_{\bar{x}_3}^{x_3} b_3(\zeta)\mathrm{d}\zeta - (x_3 - \bar{x}_3)(\sigma_{13,1}(\bar{x}_3) + \sigma_{23,2}(\bar{x}_3)) + \sigma_{33}(\bar{x}_3). \tag{2c}$$

In Eqs. (2a)–(2c), the integral constants should be chosen to fulfill the boundary conditions at the top or bottom surface $\bar{x}_3$ (see, [43] for further details).

Hereinafter, Einstein's notation on repeated indices is used, as well as the convention for which indices in Greek letters take values {1,2}. Accordingly, in Eq. (2) the derivatives of the in-plane stress components can be evaluated as

$$\sigma_{\alpha\beta,\gamma} = \mathbb{C}^{(k)}_{\alpha\beta\zeta\eta}(x_3)(-x_3\kappa_{\zeta\eta,\gamma}) = \mathbb{C}^{(k)}_{\alpha\beta\zeta\eta}(x_3)(-x_3 w_{,\zeta\eta\gamma}), \tag{3a}$$

$$\sigma_{\alpha\beta,\gamma\delta} = \mathbb{C}^{(k)}_{\alpha\beta\zeta\eta}(x_3)(-x_3\kappa_{\zeta\eta,\gamma\delta}) = \mathbb{C}^{(k)}_{\alpha\beta\zeta\eta}(x_3)(-x_3 w_{,\zeta\eta\gamma\delta}), \tag{3b}$$

where $\kappa_{\gamma\delta} = w_{,\gamma\delta}$ are the curvatures of the deflected plate mid-surface, while $\mathbb{C}^{(k)}_{\alpha\beta\zeta\eta}$ are the material tensor components for the (k)-th layer. In Eqs. (3a) and (3b), we remark that the post-processing step involves second derivatives of the plate curvatures $\kappa_{\zeta\eta,\gamma\delta}$, thereby requiring the displacement solution to be at least C^3-continuous. Such a continuity can be achieved in a straightforward manner by means of IgA. Finally, we highlight that the material tensor components $\mathbb{C}^{(k)}_{\alpha\beta\gamma\delta}$ need to be transformed in the basis of the *problem coordinate* system $\{\boldsymbol{E}_\alpha\}$ [31] as

$$\mathbb{C}^{(k)}_{\alpha\beta\gamma\delta} = D_{\alpha a} D_{\beta b} D_{\gamma c} D_{\delta d} \mathbb{C}^{(k)}_{abcd}, \tag{4}$$

where $\mathbb{C}^{(k)}_{abcd}$ are the material tensor components in the basis of the *principal material coordinates* $\{\boldsymbol{e}_a\}$ (namely $\boldsymbol{e}_1$, $\boldsymbol{e}_2$, and $\boldsymbol{e}_3$ are taken as the fiber, matrix, and normal directions, respectively) which find a convenient representation adopting Voigt's notation as

$$\mathbb{C}^{(k)} = \begin{bmatrix} \mathbb{C}_{11} & \mathbb{C}_{12} & 0 \\ & \mathbb{C}_{22} & 0 \\ & \text{symm.} & \mathbb{C}_{66} \end{bmatrix} = \begin{bmatrix} \frac{1}{E_1} & -\frac{\nu_{12}}{E_1} & 0 \\ & \frac{1}{E_2} & 0 \\ & \text{symm.} & \frac{1}{G_{12}} \end{bmatrix}^{-1}, \tag{5}$$

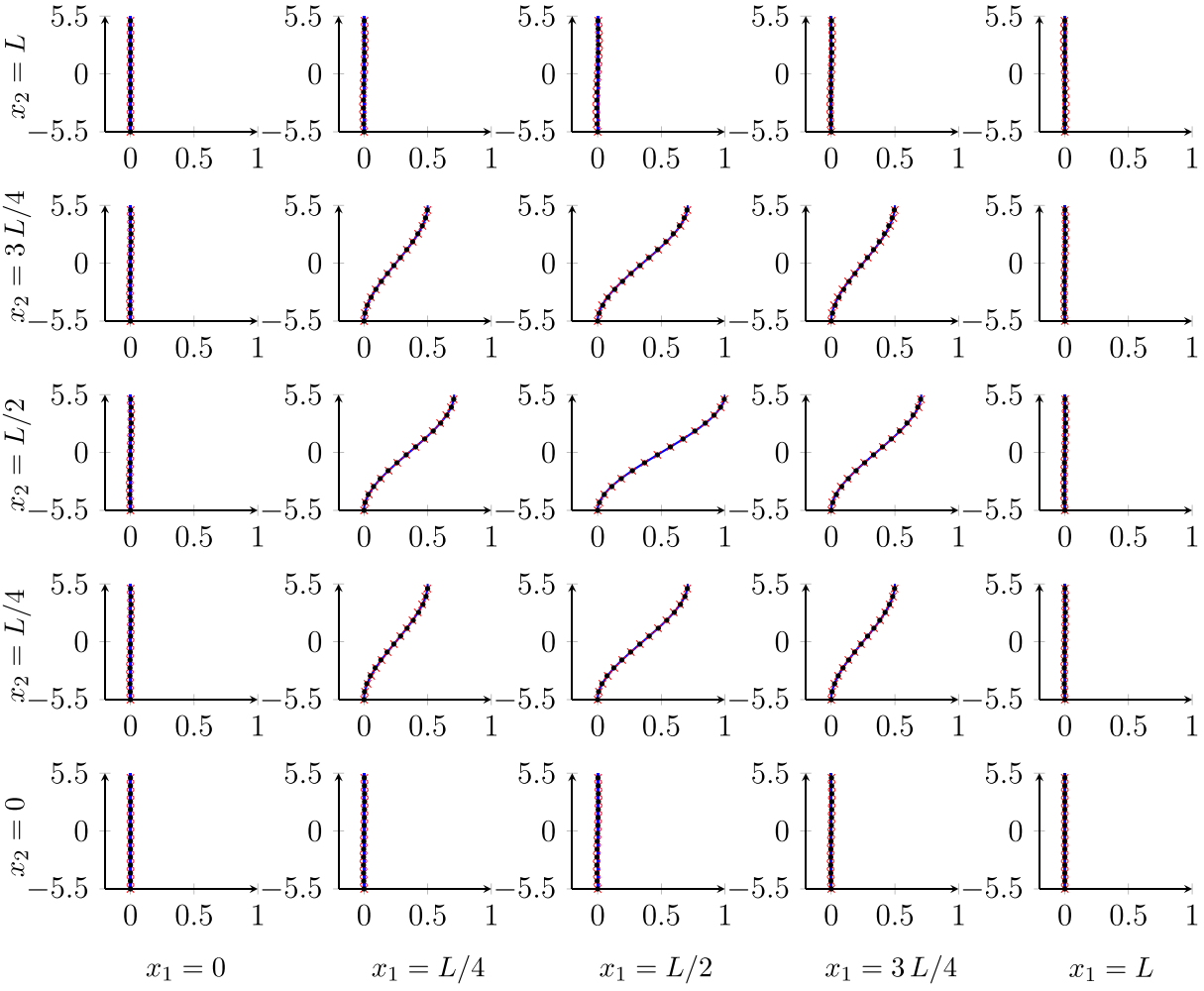

Figure 6 Through-the-thickness $\bar{\sigma}_{33}$ profiles for several in-plane sampling points. L represents the total length of the plate, that for this case is $L = 550$ mm (being $L = St$ with $t = 11$ mm and $S = 50$), while the number of layers is 11 (—— Pagano's analytical solution [49] *versus* recovered numerical solutions obtained with degree of approximation $p = q = 4$, and 14×14 knot spans: × FCM-IgA, • conforming IgA).

while $D_{\alpha a}$ are the components of the basis change operator defined as:

$$D_{\alpha a} = \boldsymbol{E}_\alpha \cdot \boldsymbol{e}_a. \tag{6}$$

3 FINITE CELL METHOD

FCM is an embedded domain method, which allows to treat complex geometrical entities in a rather simple way. The basic idea of such a method consists of embedding a complex shape domain Ω_{phys} within a fictitious domain Ω_{fict} such that the resulting domain $\Omega = \Omega_{fict} \cup \Omega_{phys}$ with $\Omega_{fict} \cap \Omega_{phys} \neq \emptyset$ can be directly discretized by means of a Cartesian grid, whose components are referred to as *finite cells* to be distinguished from traditional boundary conforming finite elements. The immersed boundary nature of such an approach requires to impose Dirichlet-type boundary conditions in a weak sense, since no boundary-conforming elements are usually present. We refer to [47] for further details.

The out-of-plane stress recovery formulation presented in Section 2 has to be modified accordingly as follows:

$$\sigma_{13}(x_3) = -\int_{\bar{x}_3}^{x_3} \alpha(\sigma_{11,1}(\zeta) + \sigma_{12,2}(\zeta) + b_1(\zeta))\mathrm{d}\zeta + \alpha\sigma_{13}(\bar{x}_3), \tag{7a}$$

$$\sigma_{23}(x_3) = -\int_{\bar{x}_3}^{x_3} \alpha(\sigma_{12,1}(\zeta) + \sigma_{22,2}(\zeta) + b_2(\zeta))\mathrm{d}\zeta + \alpha\sigma_{23}(\bar{x}_3), \tag{7b}$$

$$\sigma_{33}(x_3) = \int_{\bar{x}_3}^{x_3} \alpha\left[\int_{\bar{x}_3}^{\zeta} (\sigma_{11,11}(\xi) + \sigma_{22,22}(\xi) + 2\sigma_{12,12}(\xi) + b_{1,1}(\xi) + b_{2,2}(\xi))\mathrm{d}\xi\right]\mathrm{d}\zeta - \int_{\bar{x}_3}^{x_3} \alpha b_3(\zeta)\mathrm{d}\zeta - \alpha(x_3 - \bar{x}_3)(\sigma_{13,1}(\bar{x}_3) + \sigma_{23,2}(\bar{x}_3)) + \alpha\sigma_{33}(\bar{x}_3), \tag{7c}$$

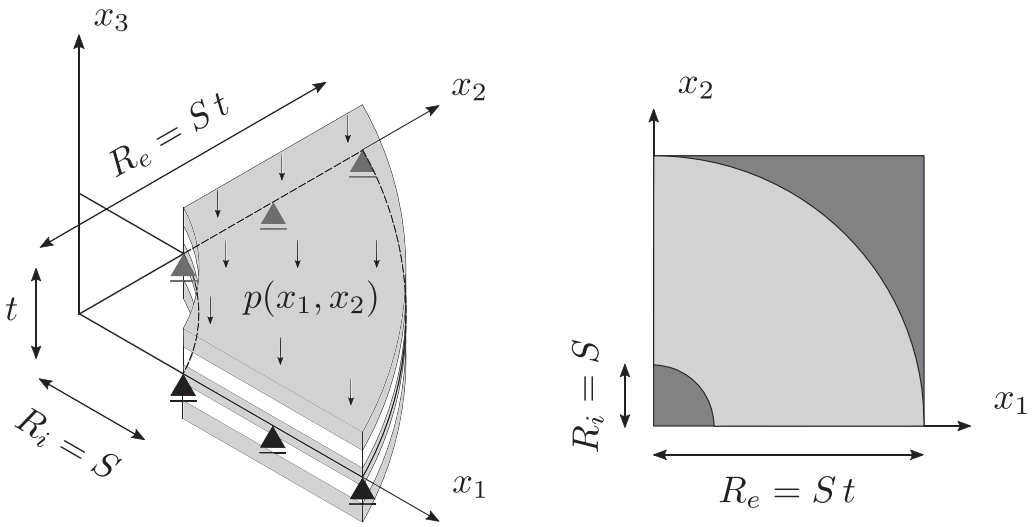

(a) Multilayered conforming quarter of annulus.

(b) Immersed *versus* conforming geometry.

Figure 7 Quarter of annulus problem setup.

where α is a discrete parameter defined as

$$\alpha = \begin{cases} 1 & \text{in } \Omega_{phys}, \\ \delta & \text{in } \Omega_{fict} \backslash \Omega_{phys}. \end{cases} \tag{8}$$

The value of the parameter δ should be zero but, for practical applications, it is set to be within the interval $[10^{-14}, 10^{-10}]$; this choice is necessary to avoid ill-conditioning of the linear system. The extended domain Ω is then discretized with a simple Cartesian grid, where each cell of the grid defines either a local support for the shape functions (as in classical FEM) or a knot span (as in conforming IgA).

In each cell the field variable w can be approximated using the extension

$$w \approx w_h = \sum_{i=1}^{p+1} \psi_i \tilde{w}_i, \tag{9}$$

where p is the maximum polynomial order of the $i-th$ shape function ψ_i and $\tilde{w}_i$ is the corresponding DOF. Different choice of the Ansatz space of the shape functions are possible for FCM; in the following, we employ NURBS basis functions [1] as basis for the analysis, i.e. we adopt the so-called IgA-version of the FCM [48].

4 NUMERICAL RESULTS

In this section, we discuss the results obtained with the previously described methodology for two classical numerical tests, namely the Pagano's benchmark and the problem of a quarter of annulus with an uniform distributed load.

4.1 Pagano's benchmark

The first numerical example is the well-known Pagano's problem as depicted in Fig. 1a, for which an analytical solution is available [49]. The problem coefficients are reported in Table 1, the material parameters in Table 2, and the distributed external load is defined as

$$q(x_1, x_2) = q_0 \sin\left(\frac{\pi x_1}{L}\right) \sin\left(\frac{\pi x_2}{L}\right),$$

where $q_0 = 1$ MPa. The FCM-IgA discretization is obtained by simply extending the patch length by a factor 1/3 in both directions, i.e. the patch length of the immersed domain is $L_{FCM} = 733.315$ mm (see Fig. 1b). All results hereinafter in terms of stress profiles are normalized according to the slender parameter S and the maximum external load q_0 as

$$\bar{\sigma}_{ij} = \frac{\sigma_{ij}}{q_0 S^2} \qquad i, j = 1, 2, \tag{10a}$$

$$\bar{\sigma}_{i3} = \frac{\sigma_{i3}}{q_0 S} \qquad i = 1, 2, \tag{10b}$$

$$\bar{\sigma}_{33} = \frac{\sigma_{33}}{q_0}. \tag{10c}$$

In Fig. 2, we present the in-plane solution profiles computed with $p = q = 4$ and 14×14 knot spans at a point of the plate domain $P = [0.25L, 0.25L]$. The normalized stresses obtained with an FCM-IgA approach prove in all cases to accurately capture the in-plane behavior of the structure also at the interface level where discontinuities in the solution are typically observed. Similar results can also be found in the literature making us confident of the effectiveness of the proposed approach (see, e.g. [50, 51]).

The plot in Fig. 3 shows instead the L^2 relative error convergence with respect to the analytical solution of the FCM-IgA discretization at the same sampling point for three different choices of in-plane approximation degrees: $p = q = 3$, $p = q = 4$, and $p = q = 6$. In the interlaminar shear stress convergence plots, a cubic in-plane approximation exhibits a pronounced oscillating behavior and high errors for the considered levels of refinement. This is most likely due to the minimum inter-element continuity in the in-plane stress derivatives. This loss of information is even more evident in the recovery of σ_{33} which provides a

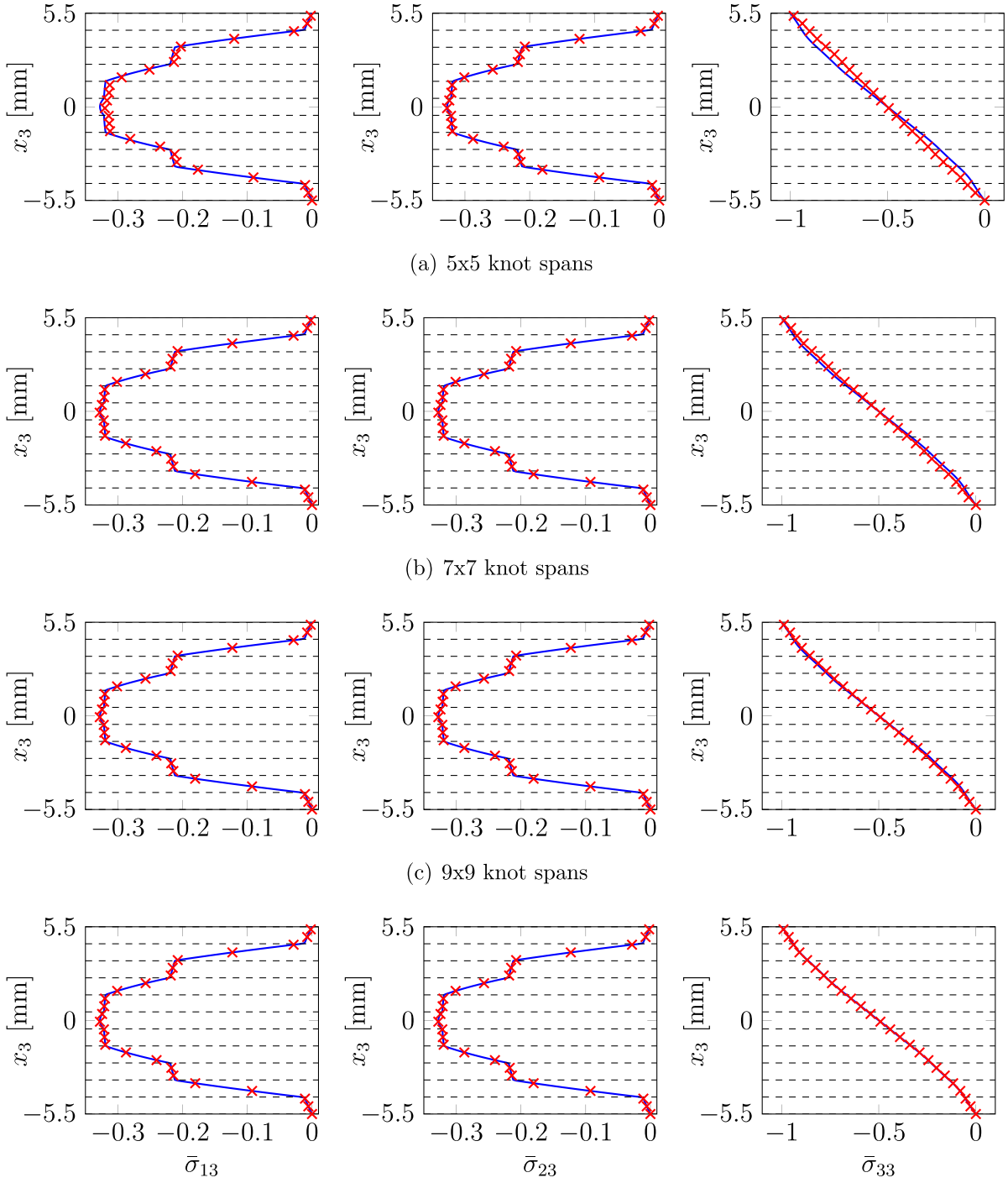

Figure 8 Post-processed interlaminar stress profiles for the quarter of annulus problem evaluated at $x_1 = 0.75\,R_e$, $x_2 = \pi/4$. Quarter of annulus plate case with 11 layers and radius-to-thickness ratio $S = 50$ (—— conforming reference solution obtained with $p = q = 6$, and 27x27 control points, × FCM-IgA computed with $p = q = 4$ and increasing number of knot spans, i.e. $5 \times 5, 7 \times 7, 9 \times 9, 11 \times 11$).

constant error around 10%. For this reason, we recommend adopting at least a quartic in-plane approximation. In fact, using $p = q = 4$, we obtain a quite high relative error (approx. 8%) for the σ_{13} and σ_{23} components only when the coarsest grid (3×3 knot spans) is employed, while such an error suddenly drops and then keeps oscillating around 1% for all three out-of-plane stress components. With $p = q = 6$, instead, even adopting the coarsest mesh of 3×3 knot spans, the relative error is steadily around 1% for σ_{13} and σ_{23}, whereas it is oscillating around 0.2% for σ_{33}. Since a similar behavior has been observed also for a conforming IgA discretization (cfr. [39]), we assume such an error associated to the out-of-plane stress recovery procedure and not to the immersed boundary nature of the numerical solution.

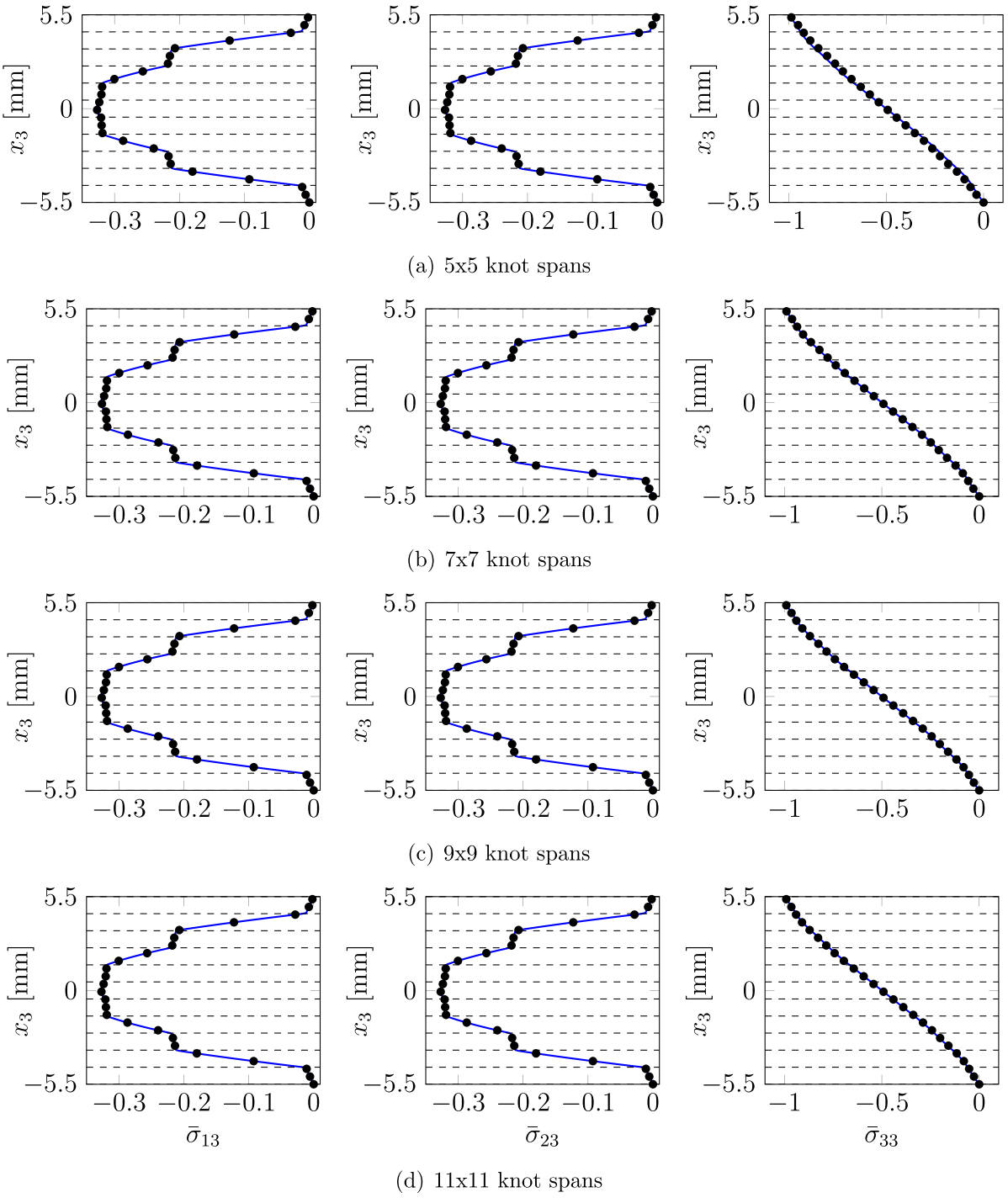

Figure 9 Post-processed interlaminar stress profiles for the quarter of annulus problem evaluated at $x_1 = 0.75\,R_e$, $x_2 = \pi/4$. Quarter of annulus plate case with 11 layers and radius-to-thickness ratio $S = 50$ (▬ conforming reference solution obtained with $p = q = 6$, and 27x27 control points, • FCM-IgA computed with $p = q = 6$ and increasing number of knot spans, i.e. $5 \times 5, 7 \times 7, 9 \times 9, 11 \times 11$).

The above observation is further validated by the results reported in Figs. 4–6, where the analytical, conforming IgA, and FCM-IgA out-of-plane stress solutions are reported at different sampling points. It can be observed that the analytical solution is well approximated by both conforming IgA and FCM-IgA discretizations showing negligible differences between them. In particular, the point-wise error in the displacement solution within the physical domain between the conforming and the immersed solutions is in the order of 10^{-6}.

4.2 Quarter of annulus

As a second numerical example, we consider a more complex geometry, namely the multilayered quarter of annulus depicted in Fig. 7a, setting the total thickness $t = 11$ mm and the

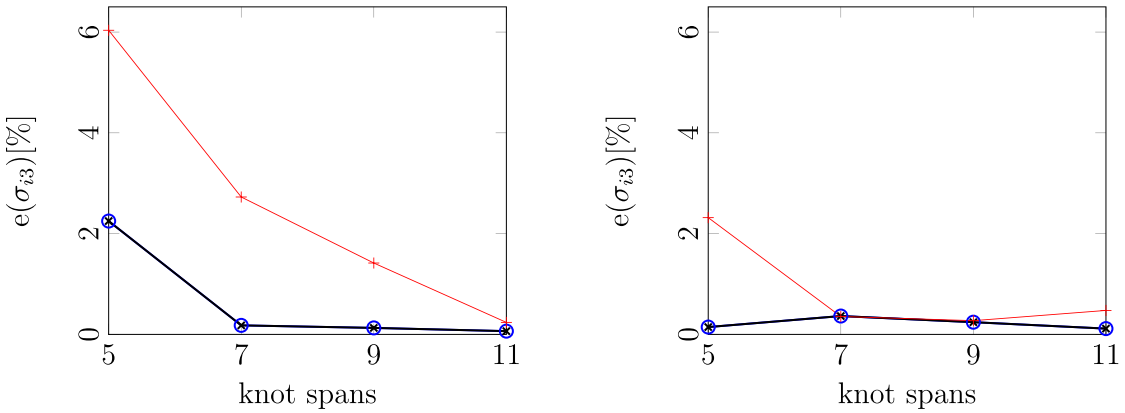

(a) 11 layers, $S = 50$, $p = q = 4$ (b) 11 layers, $S = 50$, $p = q = 6$

Figure 10 L^2 relative percentage error evaluation $(\mathrm{e}(\sigma_{i3})[\%], i = 1, 2, 3)$ at $x_1 = 0.75\,R_e$, $x_2 = \pi/4$. Different number of knot spans (i.e. $5 \times 5, 7 \times 7, 9 \times 9, 11 \times 11$) are investigated for a number of layers equal to 11 and $S = 50$ ($\mathrm{e}(\sigma_{13})[\%]$ —o—, $\mathrm{e}(\sigma_{23})[\%]$ —x—, $\mathrm{e}(\sigma_{33})[\%]$ —+—).

radius-to-thickness ratio $S = 50$, such that the internal radius $R_i = t$ [mm] and the external one $R_e = S\,t$ [mm]. The structure features a cross-ply distribution of $N_l = 11$ layers, namely a $90^\circ/0^\circ/\ldots$ stacking sequence from the bottom to the top of the plate. For each ply the material parameters remain the same as in the previous example, whereas the quarter of annulus is subjected to a constant distributed external load $p(x_1, x_2) = -1$ MPa and is simply supported at the straight edges while the curved edges are free. In this case, the FCM-IgA discretization is easily obtained by immersing the quarter of annulus geometry into a squared-patch of side $L = R_e$ such that the straight edges of the conforming geometry partially coincide with two of the patch sides (see Fig. 7b).

For this example, all numerical simulations are carried out for a sampling point located at $x_1 = 0.75\,R_e$, $x_2 = \pi/4$ using a radius-to-thickness ratio $S = 50$ and 11 layers, whereas as a reference solution we take a conforming IgA discretization comprising an in-plane degree of approximation $p = q = 6$ and 27×27 control points. Figs 8 and 9 report the recovered interlaminar stresses obtained starting from a displacement-based FCM-IgA solution for in-plane degrees of approximation $p = q = 4$ and $p = q = 6$ for several in-plane discretizations comprising 5×5, 7×7, 9×9, and 11×11 knot spans, respectively. In all cases, we are able to accurately capture the out-of-plane behavior of the plate, except in the case of the coarsest FCM-IgA discretizations.

In Fig. 10, we assess the validity of the method in terms of L^2 relative error convergence through the laminate thickness for the FCM-IgA discretizations with respect to the reference conforming IgA solution at $x_1 = 0.75\,R_e$, $x_2 = \pi/4$ and investigating $p = q = 4$ and $p = q = 6$. For a degree of approximation $p = q = 4$, the post-processing approach provides errors in the order of 0.2% for interlaminar shear stresses and rather coarse meshes (i.e. 7×7 knot spans), while for the recovery of σ_{33} we need to account for the finest discretization considered in this example (i.e. 11×11 knot spans) to attain the same level of accuracy as for σ_{13} and σ_{23}. This behavior may be expected as the recovery of σ_{33} component involves higher order derivatives than for the post-processing of the interlaminar shear stresses. Thus, these results suggest that using $p = q = 4$ and 11×11 knot spans seems to be a reasonable choice to correctly reproduce the complete stress state for this plate example. Instead, taking into account a degree of approximation $p = q = 6$, the error evolution highlights that the modeling error given by the recovery dominates over the approximation one.

5 CONCLUSIONS

In the present work, we have combined the IgA stress recovery procedure for CLPT and the FCM in order to provide an organic numerical framework able to treat complex geometrical entities in a simple yet effective way. The presented results show the effectiveness of such an approach, which is able to return approximately the same accuracy achieved by means of conforming IgA meshes using a more simple and flexible geometrical treatment.

The prospective of the present work are manifold: firstly, the recovery stress procedure can be extended to more complex variational formulations (e.g. Kirchhoff-Love shells); secondly, the FCM implementation can be enriched by including trimmed surface treatment (see, [16]) and more efficient adaptive integration schemes (e.g. the smart octtree approach presented in [52]); finally, the approach can be extended to include more complex material models, such as plastic or visco-plastic models.

ACKNOWLEDGEMENTS

This work was partially supported by the Italian Ministry of University and Research (MUR) through the PRIN project "XFAST-SIMS: Extra fast and accurate simulation of complex structural systems" (No. 20173C478N), within the program Progetti di ricerca di Rilevante Interesse Nazionale (PRIN). Such a support is gratefully acknowledged.

REFERENCES

1. Cottrell JA, Hughes TJR, Bazilevs Y. *Isogeometric Analysis: Toward Integration of CAD and FEA*. UK: Wiley, 2009.

2. Hughes TJR, Cottrell JA, Bazilevs Y. Isogeometric analysis: CAD, finite elements, NURBS, exact geometry and mesh refinement. *Computer Methods in Applied Mechanics and Engineering* 2005;**194**:4135–4195.
3. Cottrell JA, Hughes TJR, Reali A. Studies of refinement and continuity in isogeometric structural analysis. *Computer Methods in Applied Mechanics and Engineering* 2007;**196**:4160–4183.
4. da Veiga LB, Buffa A, Sangalli G, Vázquez R. Mathematical analysis of variational isogeometric methods. *Acta Numerica* 2014;**23**:157–287.
5. International Conference on Isogeometric Analysis. *Special Issue on Isogeometric Analysis: Progress and Challenges. Computer Methods in Applied Mechanics and Engineering*. Pavia, Italy: Elsevier, 2017.
6. Kiendl J, Hsu MC, Wu MCH, Reali A. Isogeometric Kirchhoff-Love shell formulations for general hyperelastic materials. *Computer Methods in Applied Mechanics and Engineering* 2015;**291**:280–303.
7. Kiendl J, Ambati M, Lorenzis LD, Gomez H, Reali A. Phase-field description of brittle fracture in plates and shells. *Computer Methods in Applied Mechanics and Engineering* 2016;**312**:374–394.
8. Patton A, Dufour JE, Antolín P, Reali A. Fast and accurate elastic analysis of laminated composite plates via isogeometric collocation and an equilibrium-based stress recovery approach. *Composite Structures* 2019;**225**:111026.
9. Wassermann B, Kollmannsberger S, Bog T, Rank E. From geometric design to numerical analysis: a direct approach using the finite cell method on constructive solid geometry. *Computers & Mathematics with Applications* 2017;**74**:1703–1726.
10. Antolin P, Buffa A, Martinelli M. Isogeometric analysis on V-reps: first results. *Computer Methods in Applied Mechanics and Engineering* 2019;**355**:976–1002.
11. Coradello L, Antolin P, Vázquez R, Buffa A. Adaptive isogeometric analysis on two-dimensional trimmed domains based on a hierarchical approach. *Computer Methods in Applied Mechanics and Engineering* 2020;**364**:112925.
12. Parvizian J, Düster A, Rank E. Finite cell method. *Computational Mechanics* 2007;**41**:121–133.
13. Düster A, Niggl A, Rank E. Applying the hp–d version of the FEM to locally enhance dimensionally reduced models. *Computer Methods in Applied Mechanics and Engineering* 2007;**196**:3524–3533.
14. Schillinger D, Ruess M, Zander N, Bazilevs Y, Düster A, Rank E. Small and large deformation analysis with the p- and B-spline versions of the finite cell method. *Computational Mechanics* 2012;**50**:445–478.
15. Schillinger D. The p- and B-spline versions of the geometrically nonlinear finite cell method and hierarchical refinement strategies for adaptive isogeometric and embedded domain analysis. Doctoral thesis, 2012.
16. Coradello L, D'Angella D, Carraturo M, Kiendl J, Kollmannsberger S, Rank E et al., Hierarchically refined isogeometric analysis of trimmed shells. *Computational Mechanics* 2020;**66**:431–447.
17. Peskin CS. The immersed boundary method. *Acta Numerica* 2002;**11**:479–517.
18. Kim J, Kim D, Choi H. An immersed-boundary finite-volume method for simulations of flow in complex geometries. *Journal of Computational Physics* 2001;**171**:132–150.
19. Ismail M. The fat boundary method for the numerical resolution of elliptic problems in perforated domains. *Application to 3D fluid flows*. PhD theses, Université Pierre et Marie Curie-Paris VI, France, 2004.
20. Moës N, Dolbow J, Belytschko T. A finite element method for crack growth without remeshing. *International Journal for Numerical Methods in Engineering* 1999;**46**:131–150.
21. Burman E, Claus S, Hansbo P, Larson MG, Massing A. CutFEM: discretizing geometry and partial differential equations. *International Journal for Numerical Methods in Engineering* 2015;**104**:472–501.
22. Xu F, Morganti S, Zakerzadeh R, Kamensky D, Auricchio F, Reali A et al., A framework for designing patient-specific bioprosthetic heart valves using immersogeometric fluid–structure interaction analysis. *International Journal for Numerical Methods in Biomedical Engineering* 2018;**34**:e2938.
23. Xu F, Bazilevs Y, Hsu MC. Immersogeometric analysis of compressible flows with application to aerodynamic simulation of rotorcraft. *Mathematical Models and Methods in Applied Sciences* 2019;**29**:905–938.
24. Kamensky D, Evans JA, Hsu MC. Stability and conservation properties of collocated constraints in immersogeometric fluid-thin structure interaction analysis. *Communications in Computational Physics* 2015;**18**:1147–1180.
25. Varduhn V, Hsu MC, Ruess M, Schillinger D. The tetrahedral finite cell method: higher-order immersogeometric analysis on adaptive non-boundary-fitted meshes. *International Journal for Numerical Methods in Engineering* 2016;**107**:1054–1079.
26. Hsu MC, Kamensky D, Xu F, Kiendl J, Wang C, Wu MC et al., Dynamic and fluid–structure interaction simulations of bioprosthetic heart valves using parametric design with T-splines and Fung-type material models. *Computational Mechanics* 2015;**55**:1211–1225.
27. Wei X, Marussig B, Antolin P, Buffa A. Immersed boundary-conformal isogeometric method for linear elliptic problems. *Computational Mechanics* 2021;**68**:1385–1405.
28. Antolin P, Buffa A, Puppi R, Wei X. Overlapping multipatch isogeometric method with minimal stabilization. *SIAM Journal on Scientific Computing* 2021;**43**:A330–A354.
29. Nitti A, Kiendl J, Reali A, De Tullio MD. An immersed-boundary/isogeometric method for fluid-structure interaction involving thin shells. *Computer Methods in Applied Mechanics and Engineering* 2020;**364**:112977.
30. Gibson RF. *Principles of Composite Material Mechanics*. New York, USA: McGraw-Hill, 1994.
31. Reddy JN. *Mechanics of Laminated Composite Plates and Shells: Theory and Analysis* (2nd Ed.). USA: CRC Press, 2003.
32. Neveu F, Castanié B, Olivier P. The GAP methodology: a new way to design composite structures. *Materials & Design*. 2019;**172**:107755.
33. Mittelstedt C, Becker W. Free-edge effects in composite laminates. *Applied Mechanics Reviews* 2007;**60**:217–245.
34. Sridharan S. *Delamination Behaviour of Composites*. Woodhead Publishing, 2008.
35. Carrera E, Cinefra M, Petrolo M, Zappino E. *Finite Element Analysis of Structures through Unified Formulation*. John Wiley & Sons, 2014.
36. Carrera E. Theories and finite elements for multi-layered, anisotropic, composite plates and shells. *Archives of Computational Methods in Engineering* 2002;**9**:87–140.
37. Liew KM, Pan ZZ, Zhang LW. An overview of layerwise theories for composite laminates and structures: Development, numerical implementation and application. *Composite Structures* 2019;**216**:240–259.
38. Li D. Layerwise theories of laminated composite structures and their applications: a review. *Archives of Computational Methods in Engineering* 2021;**28**:577–600.
39. Patton A, Antolín P, Dufour JE, Kiendl J, Reali A. Accurate equilibrium-based interlaminar stress recovery for isogeometric laminated composite Kirchhoff plates. *Composite Structures* 2021;**256**:112976.
40. Daghia F, de Miranda S, Ubertini F, Viola E. A hybrid stress approach for laminated composite plates within the first-order shear deformation theory. *International Journal of Solids and Structures* 2008;**45**:1766–1787.
41. Engblom JJ, Ochoa OO. Through-the-thickness stress predictions for laminated plates of advanced composite materials. *International Journal for Numerical Methods in Engineering* 1985;**21**:1759–1776.
42. Pryor CW, Barker RM. A finite-element analysis including transverse shear effects for applications to laminated plates. *AIAA Journal* 1971;**9**:912–917.
43. Dufour JE, Antolín P, Sangalli G, Auricchio F, Reali A. A cost-effective isogeometric approach for composite plates based on a stress recovery procedure. *Composites Part B: Engineering* 2018;**138**:12–18.

44. Patton A, Antolín P, Kiendl J, Reali A. Efficient equilibrium-based stress recovery for isogeometric laminated curved structures. *Composite Structures* 2021;**272**:113975.
45. Chiappa A, Groth C, Reali A, Biancolini ME. A stress recovery procedure for laminated composite plates based on strong-form equilibrium enforced via the RBF Kansa method. *Composite Structures* 2020;**244**:112292.
46. Sun CT, Li S. Three-dimensional effective elastic constants for thick laminates. *Journal of Composite Materials* 1988;**22**:629–639.
47. Kollmannsberger S, Özcan A, Baiges J, Ruess M, Rank E, Reali A. Parameter-free, weak imposition of Dirichlet boundary conditions and coupling of trimmed and non-conforming patches. *International Journal for Numerical Methods in Engineering* 2015;**101**:670–699.
48. Schillinger D, Dedé L, Scott MA, Evans JA, Borden MJ, Rank E et al. An isogeometric design-through-analysis methodology based on adaptive hierarchical refinement of NURBS, immersed boundary methods, and T-spline CAD surfaces. *Computer Methods in Applied Mechanics and Engineering* 2012;**249-252**:116–150.
49. Pagano NJ. Exact solutions for rectangular bidirectional composites and sandwich plates. *Journal of Composite Materials* 1970;**4**:20–34.
50. Liu N, Jeffers AE. Isogeometric analysis of laminated composite and functionally graded sandwich plates based on a layerwise displacement theory. *Composite Structures* 2017;**176**:143–153.
51. Liu N, Johnson EL, Rajanna MR, Lua J, Phan N, Hsu MC. Blended isogeometric Kirchhoff–Love and continuum shells. *Computer Methods in Applied Mechanics and Engineering* 2021;**385**:114005.
52. Kudela L, Zander N, Kollmannsberger S, Rank E. Smart octrees: accurately integrating discontinuous functions in 3D. *Computer Methods in Applied Mechanics and Engineering* 2016;306:406–426.